ELSEVIER

Contents lists available at ScienceDirect

Microporous and Mesoporous Materials

journal homepage: www.elsevier.com/locate/micromeso





Synthesis of high-surface area tungstated zirconia by atomic layer deposition on mesoporous silica

Ching-Yu Wang, Ohhun Kwon, Raymond J. Gorte, John M. Vohs

Department of Chemical and Biomolecular Engineering, University of Pennsylvania, Philadelphia, PA, 19104, USA

ARTICLE INFO

Keywords: Atomic layer deposition (ALD) Mesoporous material Solid acid catalysis Brønsted acid site

ABSTRACT

Atomic layer deposition (ALD) was used to prepare $\rm ZrO_2$ films on the surface of the mesoporous silica, SBA-15, and to modify the surface of these films with $\rm WO_3$ in order to form tungstated zirconia. Adsorption-desorption isotherms, pore size distributions, and transmission electron microscopy demonstrated that the ALD synthesis produced zirconia films that were conformal to the SBA-15 pores. DRIFT spectroscopy of pyridine adsorbed on the tungstated-zirconia SBA-15 samples showed adsorbed pyridinium ions, confirming the presence of Brønsted-acid sites on this material, consistent with what has been reported for bulk tungstated zirconia. The ALD-synthesized, tungstated-zirconia SBA-15 was also shown to be active in the acid-catalyzed H-D exchange between toluene and $\rm D_2O$.

1. Introduction

Tungstated zirconia has properties characteristic of a solid Brønsted acid and is active for the isomerization of small alkanes, such as butane and n-propane, at relatively low temperatures [1–3]. While the structure of the active form of the catalyst is still an open question, it is clear that intimate contact between the tungsta and zirconia is required for the formation of the acid sites. It is also known that each Brønsted site consists of multiple W atoms in the form of a (WO_{χ})_n cluster, with several papers suggesting a minimum of four W per site [4,5].

An active tungstated zirconia catalyst can be produced using atomic layer deposition (ALD) to grow ultrathin WO $_3$ films on a zirconia support as demonstrated by Wang et al. [5]. This work demonstrated that both Brønsted-acid sites and redox sites were generated following deposition of WO $_3$ and that the density of each type of site could be controlled by varying the number of WO $_3$ ALD cycles. The maximum Brønsted-site concentration was achieved after 5 ALD cycles. The ability to prepare tungstated zirconia with active Brønsted-acid sites using ALD presents the exciting possibility producing high-surface-area, solid-acid catalysts in well-defined pore structures that would be difficult to produce by more conventional methods. This has motivated the present study in which we have explored the use of ALD to synthesize tungstated zirconia on a mesoporous silica, SBA-15. SBA-15 features uniform one-dimensional pores with a diameter up to 10 nm, depending on synthesis conditions, and typically has a surface area greater than 600

It should be noted that SBA-15 has previously been studied as a support for tungstated zirconia with the active phase being produced by wet infiltration of zirconium acetylacetonate and ammonium metatungstate [7]. While this synthesis method produces an active catalyst, it provides less control over the structure of the WO₃/ZrO₂ deposits, and pore blockage will likely occur at relatively low weight loadings [8]. In contrast, ALD growth of WO₃/ZrO₂ in SBA-15 has the potential to produce a much more uniform material while preserving the linear pore structure of the support. Indeed, previous studies have shown that ALD can be an effective means to grow conformal metal oxide films in the pores of mesoporous oxides, including SBA-15 [9-17]. For example, Zaera and coworkers used ALD to grow TiO2 and Al2O3 films on SBA-15 [15,16], while Pagan-Torres et al. used this approach to grow Nb₂O₃ films on this support [11]. The Zaera group did extensive characterization of the growth process and the structure of the resulting films and demonstrated that the ALD oxide films were conformal to the SBA-15, with the pore diameter decreasing systematically with the number of ALD cycles.

Here, we have explored the use of ALD to grow tungstated zirconia films in the pores of SBA-15. The deposition rate per ALD cycle for each oxide was measured and the structure of the resulting films was characterized using a combination of temperature programmed desorption-thermogravimetric analysis (TPD-TGA) of 2-propanol, transmission electron microscopy (TEM), and N_2 adsorption isotherms. The formation

E-mail address: vohs@seas.upenn.edu (J.M. Vohs).

 m^2/g [6].

^{*} Corresponding author.

of active Brønsted acid sites in the ALD-synthesized $WO_3/ZrO_2/SBA-15$ materials was confirmed using diffuse reflectance infrared Fourier transform (DRIFT) spectroscopy of adsorbed pyridine and the rate of H-D exchange between D_2O and toluene. The thermal stability of the mesoporous structure was also shown to improve after coating the structure with ZrO_2 .

2. Experimental section

SBA-15 was synthesized following a process reported in the literature [6,11]. Initially, 4.0 g of Pluronic P-123 (Sigma-Aldrich) was dissolved in 120 g of 2 M HCl solution and 30 g deionized water with stirring at 298 K for 20h. Tetraethoxysilane (TEOS, Sigma-Aldrich, 99%) was then added dropwise with stirring at 308 K until 8.5 g had been added, at which point the solution was stirred at this temperature for 20 h. The solution was then maintained at 373 K for 24 h to allow hydrolysis of the TEOS. The resulting SBA-15 precipitate was filtered, washed with deionized water, and dried at 353 K for 8 h in air. To remove the P-123 surfactant, the sample was calcined in flowing air at 773 K for 6 h with an initial ramping rate of 1 K/min. As shown in Fig. S1a, the low-angle X-ray diffraction (XRD) pattern of the as-synthesized SBA-15 contains the 100, 110, and 200 peaks that are characteristic of this material [6].

ALD of ZrO₂ and WO₃ onto the SBA-15 was performed using a homebuilt ALD system that has been described in detail previously [18–20]. Tetrakis(2,2,6,6-tetramethyl-3,5-heptanedionato)zirconium (Zr(TMHD)₄, Strem Chemicals, 99%) was used as the Zr precursor and tungsten carbonyl (W(CO)₆, Strem Chemicals, 99%) was used as the W precursor. For each ZrO₂ ALD cycle, the sample was evacuated, then exposed to Zr(TMHD)₄ vapor at 523 K for 10 min, followed by oxidation at 773 K in flowing air for 40 min. Note that this high-temperature oxidation step was required to fully oxidize the adsorbed Zr(TMHD)₄ precursor. While it is common to use ozone or an O₂ plasma for this purpose, these oxidants are ineffective on highly porous substrates where rapid quenching of radicals occurs on the external surfaces [21–23]. Throughout the paper, we denote ZrO₂-modified SBA-15 samples as XX-ZrO₂/SBA-15, where XX corresponds to the number of ZrO₂ ALD cycles.

In a WO $_3$ ALD cycle, the evacuated sample was exposed to W(CO) $_6$ vapor at 473 K for 3 min, followed by evacuation and then oxidation at the same temperature in air for 6 min. We use YY-WO $_3$ -XX-ZrO $_2$ /SBA-15 to denote samples with YY ALD cycles of WO $_3$ on the XX-ZrO $_2$ /SBA-15. The ALD growth rates of ZrO $_2$ and WO $_3$ were determined gravimetrically. The low-angle XRD pattern of a 15-ZrO $_2$ /SBA-15 sample displayed in Fig. S1a contains the peaks that are characteristic of SBA-15, demonstrating that the SBA-15 structure was maintained following ZrO $_2$ ALD. Fig. S1b shows the wide angle XRD patterns of SBA-15, 15-ZrO $_2$ /SBA-15, and 5-WO $_3$ -15-ZrO $_2$ /SBA-15. No characteristics peaks were detected in these diffraction patterns for either ZrO $_2$ or WO $_3$ which is consistent with the formation of uniform ultra-thin films.

For comparison purposes, we also synthesized a WO $_3$ -modified ZrO $_2$ powder. The ZrO $_2$ powder was synthesized by dissolving zirconyl hydrate (ZrO(NO $_3$) $_2$ ·xH $_2$ O, Sigma-Aldrich, 99%) in deionized water, followed by drying in air at 333 K for 12 h and calcining in air at 773 K for 5 h [24]. The resulting ZrO $_2$ powder had a surface area of 77 m 2 /g. WO $_3$ was deposited on the ZrO $_2$ powder using 5 ALD cycles using the procedure described above. As mentioned above, an earlier study showed that 5 ALD cycles of WO $_3$ maximized the Brønsted -site concentration of tungstated zirconia prepared by ALD [5].

 $\rm N_2$ adsorption-desorption isotherms were measured at 78 K using a Micromeritics, TriStar II Plus surface area and porosity analyzer. For these measurements, the samples were pretreated at 573 K under evacuation. Surface areas were determined using the BET method and pore-size distributions were determined from the adsorption isotherms using the Barrett-Joyner-Halenda (BJH) method. XRD patterns for each sample were obtained using Xenocs Xeuss 2.0 and Rigaku MiniFlex 6G x-ray diffractometers for 0–5 and 10–70 $^{\circ}$ 20, respectively. Transmission

electron microscopy (TEM), scanning transmission electron microscopy (STEM), and energy dispersive X-ray spectra (EDS) were performed with a JEOL JEM-F200 STEM operated at 200 kV. For these measurements, the samples were diluted in ethanol and then deposited onto carbon support films on copper grids (Electron Microscopy Sciences).

TPD-TGA was used to characterize both the structure and reactivity of the various samples. The TPD-TGA system consisted of a vacuum microbalance (CAHN 2000) equipped with a quadrupole mass spectrometer (Stanford Research Systems, RGA-100) and allowed the mass change and desorbing products to be measured simultaneously. In a TPD-TGA measurement, 20 mg of sample was loaded into the microbalance and then pretreated by heating to 823 K in a vacuum of $\sim\!10^{-8}$ Torr, then cooling to 298 K. After this, the sample was exposed to 2-propanol (Fisher Scientific, 99.9%) vapor, followed by evacuation at room temperature. The sample was then heated from 298 to 823 K at 10 K/min while measuring the mass and the desorbing species.

DRIFT spectroscopy was performed using an FTIR (Mattson, Galaxy) equipped with a diffuse-reflectance cell (Pike Technologies, DiffusIR). In each DRIFT measurement, the sample was pretreated at 523 K with flowing He for 30 min before cooling to 423 K. The sample was exposed to pyridine (Fisher Chemical, 99.9%) vapor with He as the carrier gas for 10 min and then flushed with He for 10 min. All DRIFT spectra were collected with the sample at 423 K.

H-D exchange between toluene (Fisher Chemical, 99.9%) and deuterium oxide (D_2O , Cambridge Isotope Laboratories, 99.9%) was used to confirm the formation of active Brønsted acid sites in the 15-ZrO₂/SBA-15 and 5-WO₃-15-ZrO₂/SBA-15 samples, as described previously [25]. Steady-state rate measurements were made using a microflow flow reactor packed with 30 mg of catalyst that was initially pretreated at 523 K in He for 30 min. The reaction was carried out by co-feeding 1% toluene and 1% D_2O in 20 mL/min of He at various temperatures. The products were analyzed by an online GC-MS (Shimadzu, GC-17A).

3. Results and discussion

3.1. ALD of ZrO2 and WO3 on SBA-15

The amount of ZrO2 and WO3 deposited on the SBA-15 support was determined gravimetrically. Fig. 1a shows a plot of the mass of ZrO2 deposited, normalized to the mass of the SBA-15, versus the number of ALD cycles. Note that this ratio increased nearly linearly with the number of ALD cycles. The ZrO₂ deposition rate was 0.06 g of ZrO₂ per g of SBA-15 per ALD cycle, corresponding to 4.9×10^{17} Zr atoms·m⁻²·cycle⁻¹. This growth rate is close to that reported previously for ALD of TiO2 and Nb2O3 on SBA-15 [11,16]. After 15 ZrO2 ALD cycles, the Zr coverage was 7.3 \times $10^{18} \mbox{ atoms m}^{-2}.$ To determine the Zr atom coverage to ZrO2 monolayers, one way is to use the surface density of Zr on the cubic $ZrO_2(100)$ plane, 7.5 \times 10¹⁸ atoms·m⁻². Based on this calculation, the ZrO2 coverage in the 15-ZrO2/SBA-15 sample is essentially 1 monolayer. Another way is to assume that two Si-OH groups on SBA-15 react with each Zr(TMHD)4. On the basis of the Si-OH group density on the mesoporous silica, $4.0 \times 10^{18} \, \text{Si-OH} \cdot \text{m}^{-2}$, a monolayer of ZrO_2 contains 2.0×10^{18} Zr atoms·m⁻² and the resulting coverage in the 15-ZrO₂/SBA-15 sample is 3.7 monolayers [14]. An analogous plot for the ALD growth of WO3 on a 15-ZrO2/SBA-15 sample is shown in the supporting information (Fig. S2). The amount of WO₃ deposited per ALD cycle was also constant at 3.8×10^{17} W atoms·m⁻²·cycle⁻¹ and is similar to that reported in a previous study [5].

Fig. 1b shows a plot of the surface area both normalized by the total mass and by the mass of only the SBA-15 as a function of the number of $\rm ZrO_2$ ALD cycles. Note that the total mass normalized surface area decreased from 610 m²/g to 245 m²/g with 15 ALD cycles of $\rm ZrO_2$. The SBA-15 mass-normalized values show, however, that 75% of the SBA-15 surface area was retained. These results demonstrate that the decrease of surface area is mainly associated with the increase in mass and argues

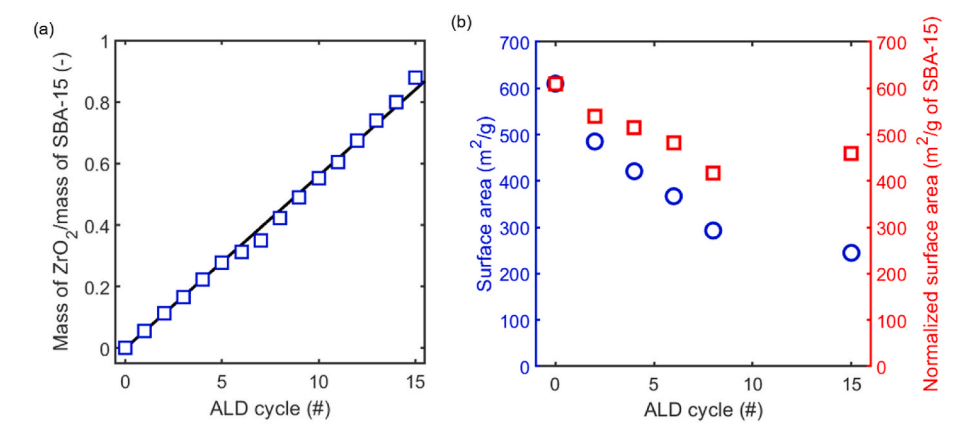


Fig. 1. (a) Mass of ZrO₂/mass of SBA-15 and (b) surface areas and normalized surface areas versus the number of ALD cycles.

against any pore blockage during ALD. The composition and surface areas of the ALD samples that were used throughout the remainder of the study, namely, 15-ZrO₂/SBA-15 and 5-WO₃-15-ZrO₂/SBA-15, are tabulated in Table 1. For comparison purposes, data for SBA-15, bulk $\rm ZrO_2$ powder, and 5-WO₃/bulk $\rm ZrO_2$ are also included in the table.

3.2. Structural characterization

 $\rm N_2$ adsorption-desorption isotherms were measured to characterize the changes in the SBA-15 pore size as a function of the number of $\rm ZrO_2$ ALD cycles. An adsorption-desorption isotherm was also measured for the 5-WO_3-15-ZrO_2/SBA-15 sample. These data are displayed in Fig. 2a and b and show the adsorption-desorption isotherms and pore size distributions, respectively. The isotherms for all samples contain a hysteresis loop that results from a difference in the onset of capillary condensation and evaporation of the $\rm N_2$ adsorbent in the linear pores in the SBA structure. Note that, in addition to the linear pores indicative of SBA-15, the pore size distribution plots show the presence of some less well-defined pores at small diameters, which we attribute to some amorphous silica that is present in our samples.

As shown in Fig. 2b, the pristine SBA-15 had a unimodal pore size distribution centered at 9.0 nm which is consistent with that reported in the literature for this material [6]. The narrow peak width in this isotherm is consistent with the SBA-15 having a relatively uniform pore structure. Fig. 2a shows that, with increasing number of ZrO₂ ALD cycles, the onset of capillary condensation shifted to lower P/P⁰ which can be attributed to a decrease in pore diameter. Note that, after 15 ZrO₂ ALD cycles (15-ZrO₂/SBA-15), the average pore size decreased to 6.6 nm; after subjecting this sample to 5 WO₃ ALD cycles (5-WO₃-15-ZrO₂/SBA-15), it was only 5.4 nm. While the pore size decreased upon oxide film growth, the shape of the hysteresis loop in the adsorption isotherms remained fairly constant, indicating that the pore structure was maintained and that the pores were uniformly covered by the metal oxide film.

To estimate the ZrO₂ film thickness, one can either use the difference

Table 1
Sample compositions and surface areas.

Material	Composition (wt%)	Surface Area (m ² /g)
SBA-15	SiO ₂ : 100	610
15-ZrO ₂ /SBA-15	ZrO ₂ : 48	245
	SiO ₂ : 52	
5-WO ₃ -15-ZrO ₂ /SBA-15	WO ₃ : 15	170
	ZrO ₂ : 41	
	SiO ₂ : 44	
Bulk ZrO ₂	ZrO ₂ : 100	77
5-WO ₃ /bulk ZrO ₂	WO ₃ : 6	65
	ZrO ₂ : 94	

between the average pore diameters of SBA-15 and that of the ALDmodified SBA-15 or calculate the thickness from the mass of added ZrO₂, using the BET surface area and assuming the film has the same density as the bulk oxide, 5.68 g/cm³. Based on the change in the pore diameter, the ZrO2 film thickness for the 15-ZrO2/SBA-15 sample was 1.2 nm; however, it was only 0.25 nm based on the mass of the deposited ZrO₂ and its bulk density. One possible contributing factor to this discrepancy is that the BJH method, which was used to calculate the pore diameters, can be imprecise for pore sizes less than ~10 nm. This is well documented in the literature where it has been shown that this method underestimates the pore size for many mesoporous materials, including SBA-type materials [26,27]. If one uses the BJH pore diameters, the film density would be less than 25% of that of the bulk value. Since for our growth procedure the film was annealed to 773 K in each ALD cycle, a temperature that should be sufficient to produce a dense ZrO2 layer, this result seems unlikely.

It should be noted, however, that in a study of the ALD growth of ${\rm TiO_2}$ on SBA-15 Ke et al. also observed a large discrepancy between the film thickness determined gravimetrically assuming a bulk density for the film, and that based on BJH pore size measurements [16]. They attributed this difference to the film nucleation process resulting in a low-density film during the initial stages of growth. While we cannot rule out this possibility, dense oxide films are routinely grown on flat substrates including oxidized silicon wafers and it is not clear why a different result would be obtained for a mesoporous silica, especially in the initial ALD cycles. It is noteworthy that, in at least some cases, ALD-deposited films as thin as 0.5 nm can show diffraction patterns consistent with bulk lattice parameters [28], a result that suggests that the ALD film densities are often similar to those of the bulk material.

The BET surface areas of the various samples are listed in Table 1. The surface area of the as-synthesized SBA-15 was 610 m^2/g and decreased to 245 m^2/g and 170 m^2/g for the 15-ZrO $_2$ /SBA-15 and 5-WO $_3$ -15-ZrO $_2$ /SBA-15 samples, respectively. Much of the decrease upon ALD oxide film growth can be attributed to the increase in the sample mass but some of the decrease must also be associated with a decrease in pore size. Even so, it is noteworthy that the surface area of the ALD-synthesized 15-ZrO $_2$ /SBA-15 (245 m^2/g) was still 3 times higher than that of the bulk ZrO $_2$ (77 m^2/g) sample.

TEM and STEM were also used to characterize the structure of the SBA-15 sample and demonstrate that the Zr in the 15-ZrO₂/SBA-15 sample was in the pores. Fig. 3a and b shows representative TEM images of SBA-15 and 15-ZrO₂/SBA-15, respectively. In the SBA-15 TEM image, both the linear pores (left region) and their arrangement in a hexagonal pattern (upper right region), which are characteristic of this material, are readily apparent. As shown in Fig. 3b, consistent with the BET results, this structure is maintained in the 15-ZrO₂/SBA-15 sample. Fig. 3c shows a representative STEM image of the 15-ZrO₂/SBA-15 sample along with EDS maps of Si and Zr from the indicated region. The Zr EDS

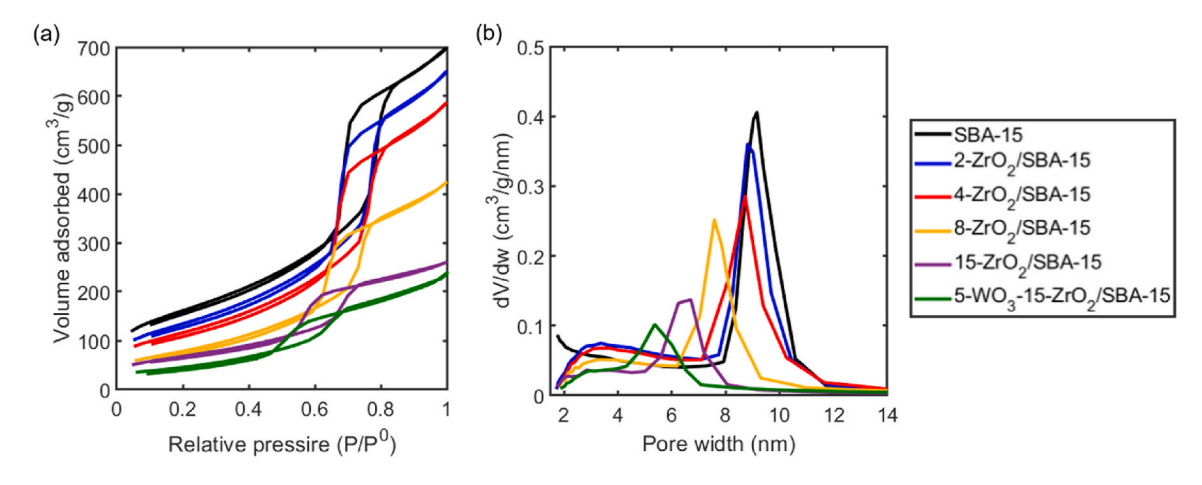


Fig. 2. (a) N₂ adsorption-desorption isotherms and (b) pore size distributions for 0 to 15 ALD cycles of ZrO₂ on SBA-15 and 5 ALD cycles of WO₃ on 15-ZrO₂/SBA-15.

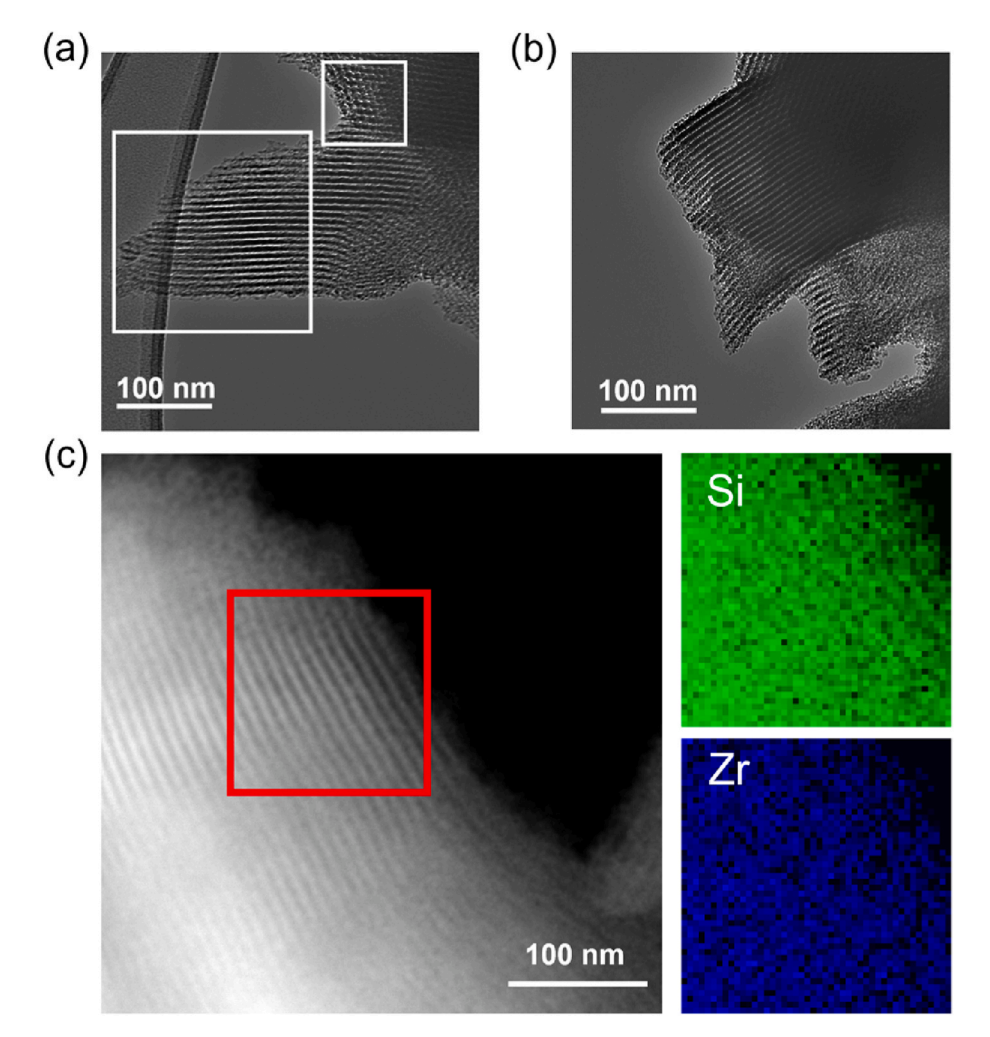


Fig. 3. TEM images of (a) SBA-15 and (b) 15-ZrO₂/SBA-15. (c) STEM image of 15-ZrO₂/SBA-15 with EDS maps of Si and Zr.

map shows that the Zr is dispersed uniformly throughout the SBA-15 which is again consistent with the adsorption results presented above.

3.3. Thermal stability

The effect of coating the pores with ZrO_2 on the thermal stability of the SBA-15 was also investigated. In these studies, the pore size

distribution, surface area, and volume of the linear pores in the SBA-15 and 15-ZrO₂/SBA-15 samples were measured after annealing each sample in air for 24 h at a series of successively higher temperatures between 1073 and 1273 K. These data are displayed in Fig. 4. We defined the volume of linear pores as the pores with width larger than 4 nm. The corresponding adsorption-desorption isotherms for each sample are provided in the supporting information (see Fig. S3).

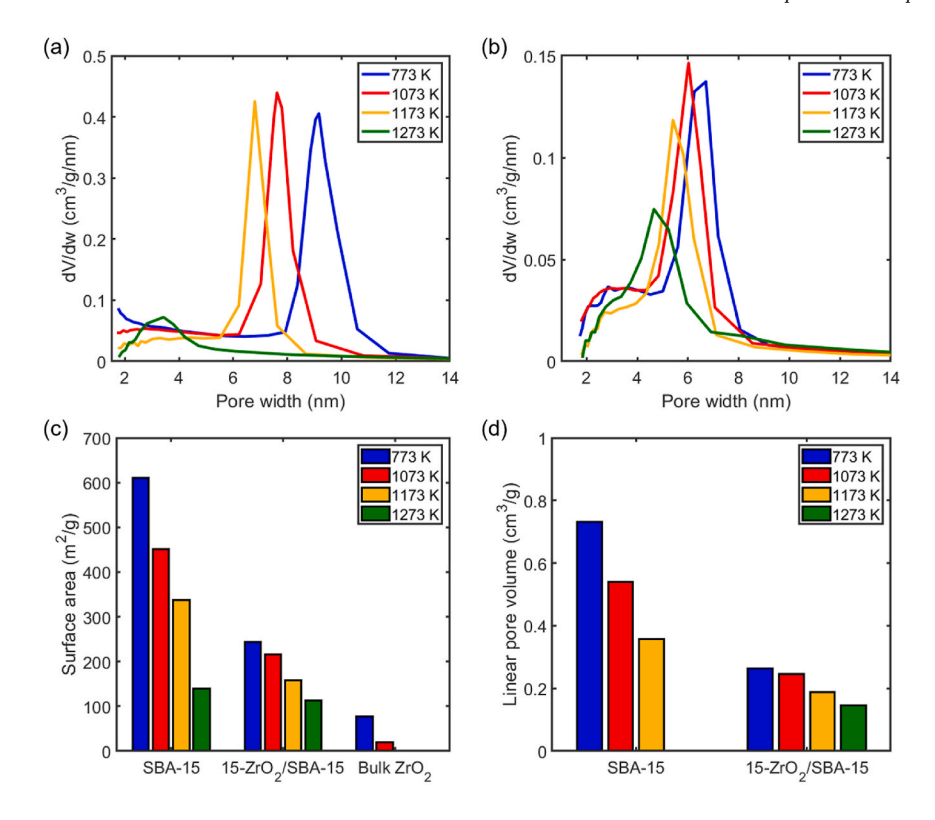


Fig. 4. Pore size distributions of (a) SBA-15 and (b) 15-ZrO₂/SBA-15 under 773–1273 K treatment. (c) Surface areas and linear pore volumes of SBA-15, 15-ZrO₂/SBA-15, and bulk ZrO₂ under 773–1273 K treatment.

As shown in Fig. 4, there were significant differences in the thermal stability of the SBA-15 and 15-ZrO $_2$ /SBA-15 samples. For SBA-15 annealing at 1073 K produced 26% and 26% decreases in the surface area and linear pore volume, respectively, while the corresponding values for 15-ZrO $_2$ /SBA-15 were only 6% and 7%. For the SBA-15, further significant decreases in surface area and pore volume occurred upon heating to 1173 K and complete collapse of the SBA-15 pore structure occurred upon heating to 1273 K, as evidenced by the

disappearance of the hysteresis loop that is characteristic of the linear pores in the adsorption isotherm (see Fig. S3a). In contrast, while some degradation did occur upon heating the $15\text{-}ZrO_2/SBA\text{-}15$ sample to 1173~K, as evidenced by decreases in surface area and pore volume (35% and 29%, respectively relative to the as-synthesized sample), it is noteworthy that, for this sample, much of the linear pore structure remained intact, even after heating to 1273~K, as evidenced by the persistence of the well-defined hysteresis loop in the adsorption

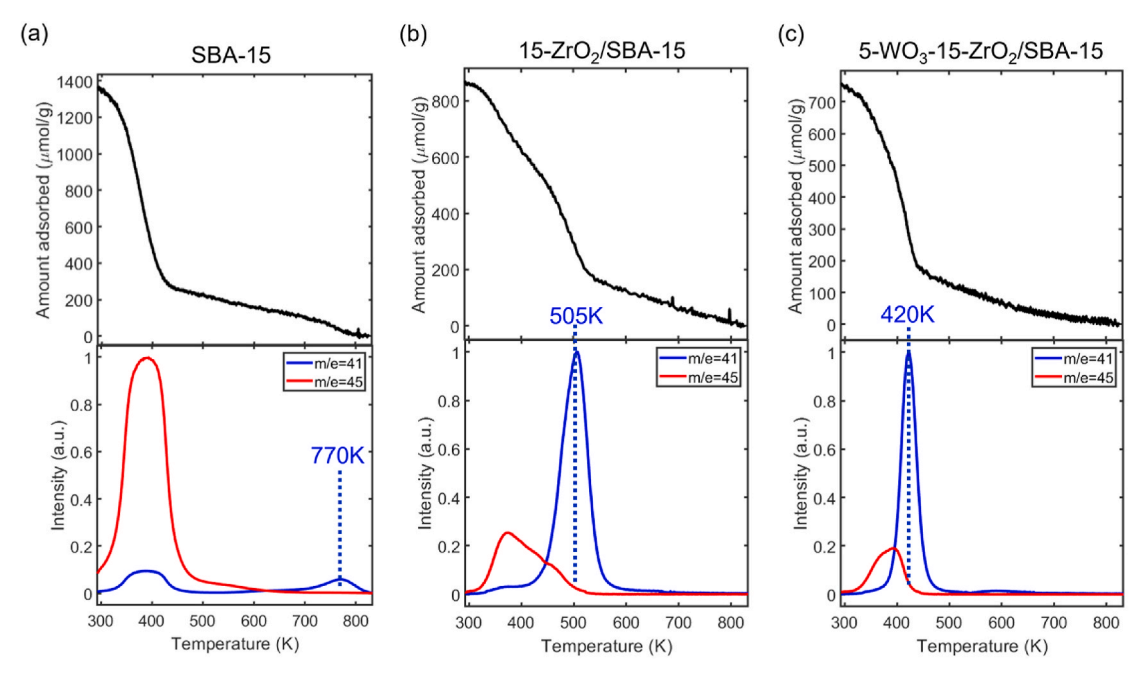


Fig. 5. 2-propanol TPD-TGA from (a) SBA-15, (b) 15-ZrO₂/SBA-15, and (c) 5-WO₃-15-ZrO₂/SBA-15. m/e = 41: propene; m/e = 41 and 45: 2-propanol.

isotherm. Somewhat surprisingly, the sample annealed at this temperature still had a linear pore volume that was 55% of that in the assynthesized sample. Even after this very harsh treatment, the $15\text{-}ZrO_2/SBA-15$ sample still had a surface area that was 1.5 times higher than that of the untreated, bulk ZrO_2 powder. These results demonstrate that coating the pores in SBA-15 with an ALD-grown ZrO_2 film produces a thermally stable, high surface area ZrO_2 .

3.4. Characterization of Lewis and Brønsted acid sites

Since 2-propanol undergoes dehydration to produce propene and water on acid sites on many metal oxide surfaces [29,30], TPD-TGA of 2-propanol was used to characterize the presence and strength of such sites on the SBA-15, 15-ZrO₂/SBA-15, and 5-WO₃-15-ZrO₂/SBA-15 samples. These experiments also provided additional insight into the uniformity of the ALD-deposited oxide films, as discussed elsewhere [5]. The TPD-TGA results for 2-propanol in SBA-15, shown in Fig. 5a, indicated that most of the alcohol (m/e = 41 and 45) desorbs intact in a large peak centered at 390 K, with a small fraction desorbing as propene (m/e = 41) in a peak centered at 770 K. This is consistent with reports in the literature for purely siliceous materials that indicate 2-propanol reacts with surface silanols to form a silvl-isopropyl ether species whose decomposition produces propene between 700 and 800 K [31,32]. Based on the TGA data, the density of sites on which this reaction takes place on SBA-15 was 130 μ mol/g (1.3 \times 10¹⁷ molecule/m²). This low coverage suggests that only a small fraction of the silanol groups on the surface react with the alcohol.

Significantly different results were obtained for the 15-ZrO₂/SBA-15 (Fig. 5b). For this sample, the 770 K propene peak observed for the bare SBA-15 was replaced by a much larger peak centered at 505 K. The absence of the 770 K peak is consistent with the ALD ZrO2 film completely covering the SBA-15 surface. The large propene peak at 505 K indicates that the ZrO2-coated sample has a higher density of active sites, in this case, exposed Zr²⁺ cations which act as Lewis acids. Based on the amount of propene produced, the Lewis-acid site density on the 15-ZrO₂/SBA-15 sample was 355 μ mol/g. This corresponds to 9×10^{17} molecules/m², a value close to that expected for a close-packed monolayer of the alcohol. Similar 2-propanol TPD-TGA results were obtained for the 5-WO₃-15-ZrO₂/SBA-15 sample, although the propene desorption feature shifted down to 420 K suggesting either stronger Lewis acidity compared to 15-ZrO2/SBA-15 or reaction on Brønsted sites that are associated with the WO3. The acid site density, 390 µmol/g, however, was similar to that of the 15-ZrO₂/SBA-15 sample.

Since WO₃-decorated ZrO₂ is reported to have Brønsted acid sites [4, 33], DRIFT spectroscopy of adsorbed pyridine was used as a probe for the presence of such sites on the 5-WO₃-15-ZrO₂/SBA-15 sample. Fig. 6 displays a DRIFT spectrum obtained after exposing this sample to pyridine at 423 K. For comparison purposes, spectra for pyridine-dosed SBA-15, 15-ZrO₂/SBA-15 and 5-WO₃/bulk ZrO₂ are also included in the figure. The spectrum for 5-WO₃/bulk ZrO₂ is similar to that reported in the literature for tungstated zirconias [5,34,35] and contains prominent adsorption peaks centered at 1600 cm⁻¹ and 1540 cm⁻¹ which have been attributed to pyridine adsorbed on Lewis acid sites and protonated pyridine (pyridinium ions) adsorbed on Brønsted-acid sites, respectively. For SBA-15, the spectrum shows no observable peak associated with Brønsted acid sites and low peak intensity for Lewis acid site, implying that SBA-15 possesses no acid site characteristics. While a prominent peak due to adsorption on Lewis acid sites is present in the spectrum for 15-ZrO₂/SBA-15, there is relatively little adsorption in the region characteristic of the pyridinium species, indicating the lack of Brønsted acid sites on this material. In contrast, a prominent peak at $1540~{\rm cm}^{-1}$ due to pyridinium ions adsorbed on Brønsted-acid sites is again present in the spectrum for 5-WO₃-15-ZrO₂/SBA-15, confirming the presence of Brønsted-acid sites on this sample. Thus, the ALD deposited WO₃/ZrO₂ layer on SBA-15 appears to have surface properties similar to that of bulk WO₃/ZrO₂.

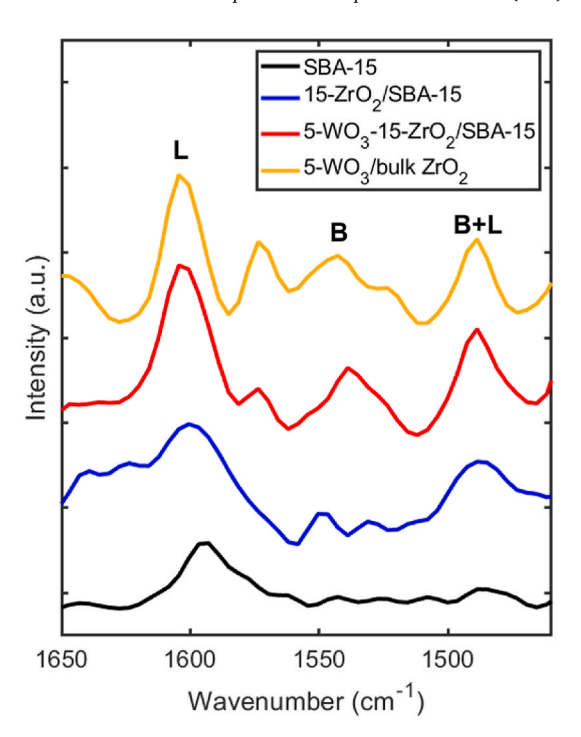


Fig. 6. DRIFT spectra with pyridine dosed SBA-15, 15-ZrO $_2$ /SBA-15, 5-WO $_3$ -15-ZrO $_2$ /SBA-15, and 5-WO $_3$ /bulk ZrO $_2$. B and L represent Brønsted and Lewis acid sites, respectively.

3.5. H-D exchange

The H-D exchange reaction between D_2O and toluene was used to further characterize the active sites on the surface of the 5-WO₃-15-ZrO₂/SBA-15 sample. H-D exchange between Brønsted sites and D_2O is known to be facile at all temperatures, but the temperature at which proton transfer occurs between a Brønsted site and toluene is strongly dependent on the strength of the Brønsted site [25]. H-D exchange is expected to occur at much lower rates on Lewis sites. Fig. 7 plots the steady-state conversion for the H-D exchange reaction as a function of temperature for the SBA-15, 15-ZrO₂/SBA-15, and 5-WO₃-15-ZrO₂/SBA-15 samples. These data show that the SBA-15 was inactive and the 15-ZrO₂/SBA-15 sample was nearly inactive, requiring temperatures

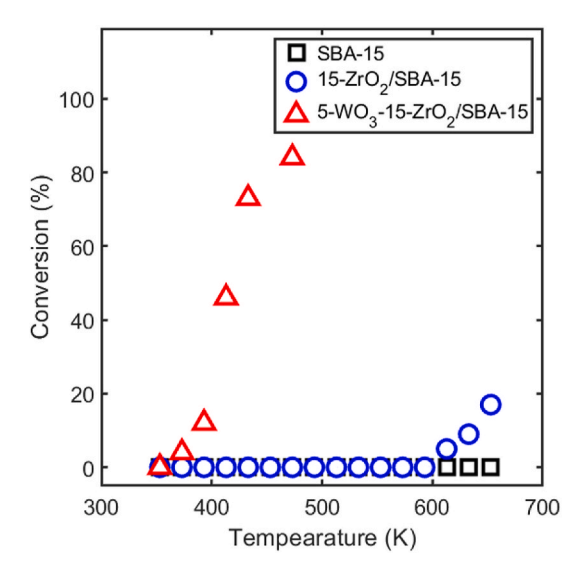


Fig. 7. Conversion for H-D exchange between toluene and D_2O as a function of temperature for SBA-15, 15-ZrO₂/SBA-15, and 5-WO₃-15-ZrO₂/SBA-15.

in excess of 600 K to produce minimal conversion. This is consistent with the lack of Brønsted acid sites on this material. Significantly different results were obtained for the $5\text{-WO}_3\text{-}15\text{-ZrO}_2/\text{SBA-}15$ sample, which was highly active for the $D_2\text{O}/\text{toluene}$ H-D exchange reaction. For this sample, the reaction onset temperature, as defined by the temperature at which 10% conversion is obtained, was 393 K; and greater than 80% conversion was obtained at 475 K. This result is consistent with the DRIFT spectra results described above and further confirms the presence of Brønsted acid sites on this catalyst.

It is useful to compare the results obtained for 5-WO $_3$ -15-ZrO $_2$ /SBA-15 with those reported previously for bulk WO $_3$ /ZrO $_2$ and transition metal substituted H-ZSM-5s by Wang et al. who used reaction conditions nearly identical to those used in the present study [5,25]. They reported that the reaction onset temperature for a 10 wt % WO $_3$ /ZrO $_2$ was 373 K which is close to that obtained here for 5-WO $_3$ -15-ZrO $_2$ /SBA-15. This demonstrates that the ALD-grown WO $_3$ /ZrO $_2$ layer in SBA-15 contains Brønsted acid sites that are similar in strength to those in a bulk tung-stated zirconia. In agreement with the previous study, the Brønsted sites in 5-WO $_3$ -15-ZrO $_2$ /SBA-15 are slightly less reactive than those in H-[Al] ZSM-5, which has a reaction onset temperature of \sim 335 K, or even H-[Fe]ZSM-5, 345 K.

4. Discussion

In this study we demonstrated the use of ALD to grow films of ZrO $_2$ in the pores of SBA-15. Upon modification with WO $_3$ this material contained Brønsted-acid sites that exhibited catalytic properties similar to those of bulk tungstated zirconia. The ALD growth process resulted in conformal films with a ZrO $_2$ growth rate was 4.9 \times 10^{17} Zr atoms·m $^{-2}$ ·cycle $^{-1}$ which remained constant for the first 15 ALD cycles. Due to the decrease in pore diameter and surface area which occurs upon ALD film growth, one might expect the growth rate per cycle to decrease with increasing cycle number once the oxide film completely covers the SBA-15 support. Note, however, that since 15 ZrO $_2$ ALD cycles produces a ZrO $_2$ film that is only slightly beyond monolayer coverage, it is likely we did not perform enough cycles to see the expected decrease in growth rate.

In addition to demonstrating the formation of active Brønsted sites for WO_3-modified 15-ZrO_2/SBA-15, this study also showed that the thermal stability of SBA-15 was greatly enhanced by coating the pores with an ALD-grown ZrO_2 film. As shown in Fig. 4, the linear pore structure was maintained after heating 15-ZrO_2/SBA-15 to 1273 K, while for the unmodified SBA-15 the pore structure completely collapsed upon heating to this temperature. This suggests that using ALD to coat the pores of mesoporous materials with a refractory oxide, such as zirconia, may be a viable strategy for producing a high-surface-area catalyst support material that can be used in applications that require high temperatures.

Finally, in addition to providing a method to produce a thermally stable, high-surface-area, tungstated zirconia (170 m²g⁻¹), a result which cannot be obtained using a bulk ZrO₂ support, these materials may have advantages for other applications. One such application is suggested by the recent study of Tennakoon et al. on the use of Pt-modified mesoporous silica for the selective hydrogenolysis of individual polymer chains in high-density polyethylene [36]. The authors of that study showed that catalytic sites that can only be accessed by diffusion of the polymer chains into mesopores were more selective to forming higher value, larger alkanes. Since Pt/WO_x/ZrO₂ has been shown to exhibit interesting properties for hydrocracking of polymers [37], the ability to produce these sites in mesopores is intriguing. Finally, recent work has shown that polymer-surface interactions can be changed significantly by modifying the surface composition of pores using ALD [38]. It is not yet clear what impact this will have on the catalytic properties but the ability to tune adsorption properties represents another variable in the catalytic toolbox.

ALD as a means to prepare catalytic materials is still in its infancy;

however, the ability to prepare materials with well-defined compositions and pore structures is intriguing. The application to mesoporous materials, demonstrated here, provides one more example of how this approach can be used to prepare interesting catalytic materials.

5. Conclusions

In this study, we demonstrated that ALD can be used to grow tung-stated zirconia on the surface of the pores in SBA-15. The observed systematic decrease in the pore diameter with the number of ALD cycles, along with 2-proponal TPD results demonstrated that the oxide films were conformal to the pore surfaces. Zirconia-coated SBA-15 was shown to enhance the thermal stability of the SBA-15 support and to have surface Lewis acid sites that are typical of zirconia. In contrast, a tungstated-zirconia modified SBA-15 that was synthesized using $15\,\rm ZrO_2$ ALD cycles followed by $5\,\rm WO_3$ ALD cycles exhibited properties consistent with the presence of surface Brønsted acid sites, including the formation of adsorbed pyridinium upon exposure to pyridine. These Brønsted sites exhibited reactivity similar to that of bulk tungstated zirconia in that they were highly active for the acid-catalyzed H-D exchange between $\rm D_2O$ and toluene.

The results of this study also further demonstrate the viability of using ALD to synthesize specific active sites on the surface of mesoporous oxides. The pore structure of these materials can be maintained while growing oxide films on their surfaces and at least in the case of zirconia, the ALD oxide film can also significantly enhance the thermal stability of the mesoporous support.

CRediT authorship contribution statement

Ching-Yu Wang: Writing – original draft, Investigation. Ohhun Kwon: Investigation. Raymond J. Gorte: Supervision. John M. Vohs: Supervision, Writing – review & editing.

Declaration of competing interest

The authors declare that they have no known competing financial interests or personal relationships that could have appeared to influence the work reported in this paper.

Acknowledgements

This work was funded by the Department of Energy, Office of Basic Energy Sciences, Chemical Sciences, Geosciences and Biosciences Division, Grant No. DE-FG02-13ER16380. The STEM work was carried out in part at the Singh Center for Nanotechnology, part of the National Nanotechnology Coordinated Infrastructure Program, which is supported by the National Science Foundation grant NNCI-1542153. The authors acknowledge Dr. Daeyeon Lee and Dr. Jaehyun Kim at the University of Pennsylvania for the help on SBA-15 synthesis. The authors acknowledge use of the Dual Source and Environmental X-ray Scattering facility operated by the Laboratory for Research on the Structure of Matter at the University of Pennsylvania (NSF MRSEC 17-20530). The equipment purchase was made possible by a NSF MRI grant (17-25969), a ARO DURIP grant (W911NF-17-1-0282), and the University of Pennsylvania.

Appendix A. Supplementary data

Supplementary data to this article can be found online at https://doi.org/10.1016/j.micromeso.2022.111821.

References

 D.G. Barton, S.L. Soled, E. Iglesia, Solid acid catalysts based on supported tungsten oxides, Top. Catal. 6 (1998) 87–99.

- [2] M. Scheithauer, T.K. Cheung, R.E. Jentoft, R.K. Grasselli, B.C. Gates, H. Knozinger, Characterization of WOx/ZrO₂ by vibrational spectroscopy and n-pentane isomerization catalysis, J. Catal. 180 (1998) 1–13.
- [3] N. Soultanidis, W. Zhou, A.C. Psarras, A.J. Gonzalez, E.F. Iliopoulou, C.J. Kiely, I. E. Wachs, M.S. Wong, Relating n-pentane isomerization activity to the tungsten surface density of WOx/ZrO₂, J. Am. Chem. Soc. 132 (2010) 13462–13471.
- [4] W. Zhou, N. Soultanidis, H. Xu, M.S. Wong, M. Neurock, C.J. Kiely, I.E. Wachs, Nature of catalytically active sites in the supported WO₃/ZrO₂ solid acid system: a current perspective, ACS Catal. 7 (2017) 2181–2198.
- [5] C. Wang, X.Y. Mao, J.D. Lee, T.M. Onn, Y.H. Yeh, C.B. Murray, R.J. Gorte, A characterization study of reactive sites in ALD-synthesized WOx/ZrO₂ catalysts, Catalysts 8 (2018) 15.
- [6] D.Y. Zhao, J.L. Feng, Q.S. Huo, N. Melosh, G.H. Fredrickson, B.F. Chmelka, G. D. Stucky, Triblock copolymer syntheses of mesoporous silica with periodic 50 to 300 angstrom pores, Science 279 (1998) 548–552.
- [7] T. Li, S.T. Wong, M.C. Chao, H.P. Lin, C.Y. Mou, S.F. Cheng, N-pentane isomerization over platinum-promoted W/Zr mixed oxides supported on mesoporous silica, Appl. Catal. A-Gen. 261 (2004) 211–219.
- [8] W. Lee, C.C. Yang, S. Cheng, Isomerization of n-pentane over platinum promoted tungstated zirconia supported on mesoporous SBA-15 prepared by supercritical impregnation, J. Chin. Chem. Soc. 68 (2021) 409–420.
- [9] Z. Gao, Y. Qin, Design and properties of confined nanocatalysts by atomic layer deposition, Accounts Chem. Res. 50 (2017) 2309–2316.
- [10] P. Cop, E. Celik, K. Hess, Y. Moryson, P. Klement, M.T. Elm, B.M. Smarsly, Atomic layer deposition of nanometer-sized CeO₂ layers in ordered mesoporous ZrO₂ films and their impact on the ionic/electronic conductivity, ACS Appl. Nano Mater. 3 (2020) 10757–10766.
- [11] Y.J. Pagan-Torres, J.M.R. Gallo, D. Wang, H.N. Pham, J.A. Libera, C.L. Marshall, J. W. Elam, A.K. Datye, J.A. Dumesic, Synthesis of highly ordered hydrothermally stable mesoporous niobia catalysts by atomic layer deposition, ACS Catal. 1 (2011) 1234–1245
- [12] Y.Q. Li, S.C. Zhao, Q.M. Hu, Z. Gao, Y.Q. Liu, J.K. Zhang, Y. Qin, Highly efficient CoOx/SBA-15 catalysts prepared by atomic layer deposition for the epoxidation reaction of styrene, Catal. Sci. Technol. 7 (2017) 2032–2038.
- [13] J. Dendooven, B. Goris, K. Devloo-Casier, E. Levrau, E. Biermans, M.R. Baklanov, K. F. Ludwig, P. Van der Voort, S. Bals, C. Detavernier, Tuning the pore size of ink-bottle mesopores by atomic layer deposition. Chem. Mater. 24 (2012) 1992–1994.
- [14] J.E. Herrera, J.H. Kwak, J.Z. Hu, Y. Wang, C.H.F. Peden, J. Macht, E. Iglesia, Synthesis, characterization, and catalytic function of novel highly dispersed tungsten oxide catalysts on mesoporous silica, J. Catal, 239 (2006) 200–211.
- [15] Z.H. Weng, Z.H. Chen, X.D. Qin, F. Zaera, Sub-monolayer control of the growth of oxide films on mesoporous materials. J. Mater. Chem. 6 (2018) 17548–17558.
- [16] W. Ke, Y. Liu, X.L. Wang, X.D. Qin, L.M. Chen, R.M. Palomino, J.P. Simonovis, I. Lee, I. Waluyo, J.A. Rodriguez, A.I. Frenkel, P. Liu, F. Zaera, Nucleation and initial stages of growth during the atomic layer deposition of titanium oxide on mesoporous silica. Nano Lett. 20 (2020) 6884–6890.
- [17] M.H. Wang, Y. Li, X.L. Gao, C.R. Liu, F. Xing, TiO2 ultrathin coating of SBA-15/Au by atomic layer deposition for enhanced catalytic performance in epoxidation of styrene, J. Phys. Chem. C 124 (2020) 10530–10540.
- [18] R.J. Huang, O. Kwon, C. Lin, R.J. Gorte, The effects of SMSI on m-Cresol hydrodeoxygenation over Pt/Nb_2O_5 and Pt/TiO_2 , J. Catal. 398 (2021) 102–108.
- [19] T.M. Onn, S.Y. Zhang, L. Arroyo-Ramirez, Y.C. Chung, G.W. Graham, X.Q. Pan, R. J. Gorte, Improved thermal stability and methane-oxidation activity of Pd/Al₂O₃ catalysts by atomic layer deposition of ZrO₂, ACS Catal. 5 (2015) 5696–5701.
- [20] T.M. Onn, M. Monai, S. Dai, E. Fonda, T. Montini, X.Q. Pan, G.W. Graham, P. Fornasiero, R.J. Gorte, Smart Pd catalyst with improved thermal stability

- supported on high-surface-area LaFeO $_3$ prepared by atomic layer deposition, J. Am. Chem. Soc. 140 (2018) 4841–4848.
- [21] G. Dingemans, C.A.A. van Helvoirt, D. Pierreux, W. Keuning, W.M.M. Kessels, Plasma-assisted ALD for the conformal deposition of SiO₂: process, material and electronic properties, J. Electrochem. Soc. 159 (2012) H277–H285.
- [22] J. Musschoot, J. Dendooven, D. Deduytsche, J. Haemers, G. Buyle, C. Detavernier, Conformality of thermal and plasma enhanced atomic layer deposition on a nonwoven fibrous substrate, Surf. Coating. Technol. 206 (2012) 4511–4517.
- [23] H.C.M. Knoops, J.W. Elam, J.A. Libera, W.M.M. Kessels, Surface loss in ozone-based atomic layer deposition processes, Chem. Mater. 23 (2011) 2381–2387.
- [24] Y.C. Ji, A. Lawal, A. Nyholm, R.J. Gorte, O.A. Abdelrahman, Dehydra-decyclization of tetrahydrofurans to diene monomers over metal oxides, Catal. Sci. Technol. 10 (2020) 5903–5912.
- [25] C. Wang, S. Li, X.Y. Mao, S. Caratzoulas, R.J. Gorte, H-D exchange of simple aromatics as a measure of brønsted-acid site strengths in solids, Catal. Lett. 148 (2018) 3548–3556.
- [26] C.G. Sonwane, S.K. Bhatia, Characterization of pore size distributions of mesoporous materials from adsorption isotherms, J. Phys. Chem. B 104 (2000) 9099–9110.
- [27] J.C. Groen, L.A.A. Peffer, J. Perez-Ramirez, Pore size determination in modified micro- and mesoporous materials. Pitfalls and limitations in gas adsorption data analysis, Microporous Mesoporous Mater. 60 (2003) 1–17.
- [28] T.Y. Cao, O. Kwon, C. Lin, J.M. Vohs, R.J. Gorte, Two-dimensional perovskite crystals formed by atomic layer deposition of CaTiO₃ on gamma-Al₂O₃, Nanomaterials (2021) 11.
- [29] S. Roy, G. Mpourmpakis, D.Y. Hong, D.G. Vlachos, A. Bhan, R.J. Gorte, Mechanistic study of alcohol dehydration on gamma-Al₂O₃, ACS Catal. 2 (2012) 1846–1853.
- [30] K. Larmier, C. Chizallet, N. Cadran, S. Maury, J. Abboud, A.F. Lamic-Humblot, E. Marceau, H. Lauron-Pernot, Mechanistic investigation of isopropanol conversion on alumina catalysts: location of active sites for alkene/ether production, ACS Catal. 5 (2015) 4423–4437.
- [31] R.J. Huang, Y. Cheng, Y.C. Ji, R.J. Gorte, Atomic layer deposition for preparing isolated Co sites on SiO₂ for ethane dehydrogenation catalysis, Nanomaterials 10 (2020) 13
- [32] M.T. Aronson, R.J. Gorte, W.E. Farneth, The influence of oxonium ion and carbenium ion stabilities on the Alcohol/H-ZSM-5 interaction, J. Catal. 98 (1986) 434-443.
- [33] V. Lebarbier, G. Clet, M. Houalla, A comparative study of the surface structure, acidity, and catalytic performance of tungstated zirconia prepared from crystalline zirconia or amorphous zirconium oxyhydroxide, J. Phys. Chem. B 110 (2006) 13905–13911.
- [34] J. Rorrer, Y. He, F.D. Toste, A.T. Bell, Mechanism and kinetics of 1-dodecanol etherification over tungstated zirconia, J. Catal, 354 (2017) 13–23.
- [35] C. Wang, T. Xie, P.A. Kots, B.C. Vance, K. Yu, P. Kumar, J. Fu, S. Liu, G. Tsilomelekis, E.A. Stach, W. Zheng, D.G. Vlachos, Polyethylene Hydrogenolysis at Mild Conditions over Ruthenium on Tungstated Zirconia, JACS Au, 2021.
- [36] A. Tennakoon, X. Wu, A.L. Paterson, S. Patnaik, Y.C. Pei, A.M. LaPointe, S. C. Ammal, R.A. Hackler, A. Heyden, Slowing II, G.W. Coates, M. Delferro, B. Peters, W.Y. Huang, A.D. Sadow, F.A. Perras, Catalytic upcycling of high-density polyethylene via a processive mechanism, Nat. Catal. 3 (2020) 893–901.
- [37] S.B. Liu, P.A. Kots, B.C. Vance, A. Danielson, D.G. Vlachos, Plastic waste to fuels by hydrocracking at mild conditions, Sci. Adv. 7 (2021) 9.
- [38] T. Ren, R. Huang, R.J. Gorte, D. Lee, Modulating interactions between molten polystyrene and porous solids using atomic layer deposition, Langmuir 37 (2021) 14520–14526.